Bull. Mater. Sci., Vol. 36, No. 4, August 2013, pp. 735–741. © Indian Academy of Sciences.

Effect of electrodeposition potential on composition and morphology of CIGS absorber thin film

N D SANG[†], P H QUANG[*], L T TU and D T B HOP

Hanoi University of Science, Vietnam National University, Hanoi, 334 Nguyen Trai, Thanh Xuan, Hanoi, Vietnam
[†]National University of Civil Engineering, 55 Giai Phong Street, Hai Ba Trung, Hanoi, Vietnam

MS received 2 December 2011; revised 23 April 2012

Abstract. **CuInGaSe (CIGS) thin films were deposited on Mo/soda-lime glass substrates by electrodeposition at different potentials ranging from −0·3 to −1·1 V vs Ag/AgCl. Cyclic voltammetry (CV) studies of unitary Cu, Ga, In and Se systems, binary Cu–Se, Ga–Se and In–Se systems and quaternary Cu–In–Ga–Se were carried out to understand the mechanism of deposition of each constituent. Concentration of the films was determined by energy dispersive spectroscopy. Structure and morphology of the films were characterized by X-ray diffraction and scanning electron microscope. The underpotential deposition mechanism of Cu–Se and In–Se phases was observed in voltammograms of binary and quaternary systems. Variation in composition with applied potentials was explained by cyclic voltammetry (CV) data. A suitable potential range from −0·8 to −1·0 V was found for obtaining films with desired and stable stoichiometry. In the post-annealing films, chalcopyrite structure starts forming in the samples deposited at −0·5 V and grows on varying the applied potential towards negative direction. By adjusting the composition of electrolyte, we obtained the desired stoichiometry of $Cu(In_{0.7}Ga_{0.3})Se_2$.**

Keywords. **Thin films; cyclic voltammetry; CuInGaSe (CIGS); solar cell; electrodeposition.**

1. Introduction

$Cu(In_{1-x}Ga_x)Se_2$ (CIGS) thin film has potential as an absorber material for solar cell application because it has a large optical absorption coefficient ($5 \times 10^5\,cm^{-1}$) which results from the direct bandgap (Bhatacharya *et al* 1998; Hermann *et al* 1998). CIGS basethin film solar cell has reached a conversion efficiency of 19·9% for laboratory-size devices fabricated from a physical vapour deposition (PVD) process (Repinst *et al* 2008). Additionally, CIGS modules have shown a long-term stability without any signs of degradation (Bhatacharya *et al* 1998; Hermann *et al* 1998). In order to make CIGS-based solar cell become more realizable, an alternative low-cost process has to be developed for the growth of high-quality CIGS absorber layer. Electrodeposition technique is potentially suitable to satisfy this requirement. Recently, there has been a number of reports on the growth of CIGS thin film using electrodeposition technique. A conversion efficiency as high as 15·4% has been achieved in the devices with CIGS film grown by electrodeposition and the composition adjusted by PVD (Bhatacharya *et al* 2000). There are two different electrochemical approaches to form CIGS films: one-step electrodeposition (Zank *et al* 1996; Kampmann *et al* 2000; Zhang *et al* 2003; Fernandez and Bhatacharya 2005; Kang *et al* 2010) that provides all constituents from the same electrolyte in a single-step and multi-step electrodeposition that deposits sequentially each constituent from different electrolytes (Friedfeld *et al* 1999; Kampmann *et al* 2003). However, one-step electrodeposition of CIGS films is rather difficult due to large difference in the values of equilibrium reduction potential for each constituent. In this technique, to achieve a desired film composition, a balancing of fluxes of the constituents can be done by adjusting the concentration in the solution as well as deposition potential. In this investigation, we study the deposition mechanism of the constituents by using cyclic voltammetry (CV) technique. We also grow CIGS thin films on Mo/soda-lime glass substrates by electrodeposition at different potentials ranging from −0·3 to −1·1 V vs Ag/AgCl. The aim of this work is mainly to find out the appropriate deposition potential in one-step electrodeposition of CIGS layer. However, based on the understanding of electrodeposition mechanism of different constituents, we also made an attempt to vary the concentration of electrolyte for matching the stoichiometry of $Cu(In_{0.7}Ga_{0.3})Se_2$.

2. Experimental

CV studies and potentiostatic electrodeposition (ED) process were carried out using a potentiostat/galvanostat model Autolab 3020 N in a three-electrode configuration where the reference electrode was Ag/AgCl, the counter electrode was a Pt spiral wire and the working electrode was

[*]Author for correspondence (phquang2711@yahoo.com)

a Mo/soda-lime glass substrate with an area of 1·5 cm^2. Mo layer was deposited by d.c. sputtering with a thickness of 1 μm and resistivity of 15 $\mu\Omega$ cm. The electrolyte bath contained 120 ml deionized water, 20 mM $CuCl_2$, 30 mM $InCl_3$, 40 mM $Ga(NO_3)_3$, 20 mM H_2SeO_3 and 350 mM LiCl. A combination of 25 mM potassium hydrogen phthalate (KHP) and 20 mM H_3SNO_3 (sulphamic acids) was used as a complexing agent. In our previous study (not published yet), we have found that this concentration of complexing agent was the best choice. pH of the solution was adjusted to 2·0 by adding drops of concentrated hydrochloric acid. CV was carried out in the range of potentials from −1·2 to 0·0 V vs Ag/AgCl at a scan rate of 20 mV/s. The first scan was in negative direction. EDs were processed at the potentials ranging from −0·3 to −1·1 V vs Ag/AgCl for 20 min. The annealing process was carried out in Ar at 550 °C for 60 min. Concentration of the films grown by ED was determined by energy dispersive spectroscopy (EDS), surface morphology was examined by scanning electron microscope (SEM) and crystallinity was examined by X-ray diffraction (XRD).

3. Results and discussion

3.1 *Voltammogram of unitary Cu, Ga, In and Se systems*

Figure 1(a) shows voltammogram of the base solution which contains only water, LiCl, KHP and H_3SNO_3. As seen in the figure, within the scan range, there is no reduction peak. It means that any reduction process does not take place in this solution. At high negative potential, the current decreases rapidly when hydrogen reduction starts occurring. Figure 1(b) presents the voltammogram of 20 mM $CuCl_2$ in the solution. In this voltammogram, we can see one weak peak at about 0·15 V, one peak at about −0·4 V and one peak at −0·9 V vs Ag/AgCl. We suggest that the peak at 0·15 V relates to the process:

$$Cu^{2+} + 2Cl^- + e^- \leftrightarrow CuCl_2^-. \quad (1)$$

Our suggestion is in agreement with the proposal by Abrantes *et al* (1995).

The peak at −0·4 V may be assigned to the process:

$$Cu^{2+} + 2e^- \leftrightarrow Cu^0. \quad (2)$$

Although it is well known that Cu deposition is a reversible process, we do not observe an oxidation peak corresponding to this reduction peak. This feature can be explained by the formation of complexation between sulphamate anions and cuprous cations. The peak at −0·9 V should be assigned to the H^+ reduction to H_2 process. All our attributions of the peaks in voltammogram of Cu unitary system are in very good agreement with those reported by Liu *et al* (2011) and Lai *et al* (2009).

Figure 1(c) presents voltammogram of the solution containing 30 mM $InCl_3$. In this figure, the reduction of In^{3+} to In reaches a maximum at −0·8 V. The voltammogram of the solution containing 40 mM $Ga(NO_3)_3$ is shown in figure 1(d). Similar to the In system, the peak at −0·9 V can be attributed to the reduction of Ga^{3+} to Ga. We can see that although the concentration of the $Ga(NO_3)_3$ is 40 mM,

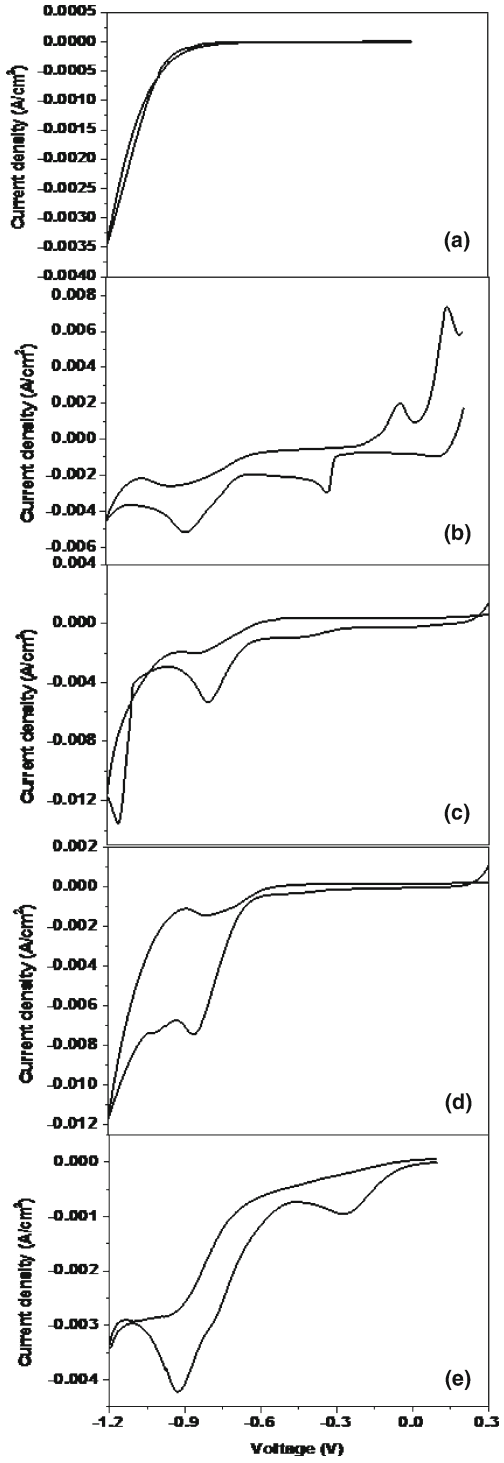

Figure 1. Voltammograms of (**a**) base solution containing water, LiCl, KHP and H_3SNO_3; (**b**) solution containing 20 mM $CuCl_2$; (**c**) solution containing 30 mM $InCl_3$; (**d**) solution containing 40 mM $Ga(NO_3)_3$ and (**e**) solution containing 20 mM H_2SeO_3.

higher than those of other constituents, the current density is rather low. It again indicates that among four elements Ga has the most negative reduction potential and therefore, is the most difficult element to deposit. The voltammogram of H_2SeO_3 presented in figure 1(e) shows two strong peaks, one at −0·3 V and the other at −0·9 V vs Ag/AgCl. The first peak is likely related to the reduction of H_2SeO_3 directly to Se, following the equation:

$$H_2SeO_3 + 4H^+ + 4e^- \leftrightarrow Se + 3H_2O. \quad (3)$$

We suggest the second peak corresponding to the complex process described by the equations:

$$H_2SeO_3 + 6H^+ + 6e^- \leftrightarrow H_2Se + 3H_2O, \quad (4)$$

$$H_2SeO^3 + 2H_2Se + 6e^- \leftrightarrow Se + 3H_2O. \quad (5)$$

This suggestion is similar to those reported by Massaccesi *et al* (1996) and Mishra and Rajeshwar (1989).

3.2 *Voltammogram of binary Cu–Se, Ga–Se and In–Se*

Figure 2(a) illustrates voltammogram of the electrolyte solution containing 20 mM $CuCl_2$ and 20 mM H_2SeO_3. The peak at −0·9 V is still assigned to the reduction processes of H_2SeO_3 which have been described in the preceding section. There are some differences between this voltammogram and those of unitary Cu and Se systems. The first notable difference is the appearance of the second peak at −0·7 V. This peak may still relate to the processes described by (4) and (5), i.e., these processes occur at a more positive potential. Liu *et al* (2011) has also observed this behaviour and attributed it to the reduction of Se to H_2Se, according to the equation:

$$Se + 2H^+ + 2e^- \leftrightarrow H_2Se. \quad (6)$$

In their report, the significant positive shift from −0·9 to −0·65 V of this reduction peak has been explained by the release of formation free energy from the reaction:

$$Se + Cu^{2+} \leftrightarrow CuSe + 2H^+. \quad (7)$$

Another notable difference is the positive shift of either the peak described by (2) or the one described by (3) from their former position where Cu^{2+} or Se^{4+} alone is reduced to the position of −0·1 V. According to Thouin *et al* (1993) the origin of this phenomenon can be attributed to the formation of a Cu–Se phase, for example:

$$2Cu^+ + H_2SeO_3 + 4H^+ + 6e^- \leftrightarrow Cu_2Se + 3H_2O, \quad (8)$$

$$Cu^{2+} + H_2SeO_3 + 4H^+ + 6e^- \leftrightarrow CuSe + 3H_2O. \quad (9)$$

Figure 2(b) shows voltammogram of solution containing 30 mM $InCl_3$ and 20 mM H_2SeO_3. By comparing this voltammogram with those of unitary In and Se systems, we can attribute the first peak at −0·3 V to the reduction of H_2SeO_3 directly to Se and the second peak at −0·8 V to the reduction of In^{3+} to In. Besides that, we can observe one peak at −0·57 V which may relate to an underpotential deposition of indium as indium selenides. This process can be described by the equation:

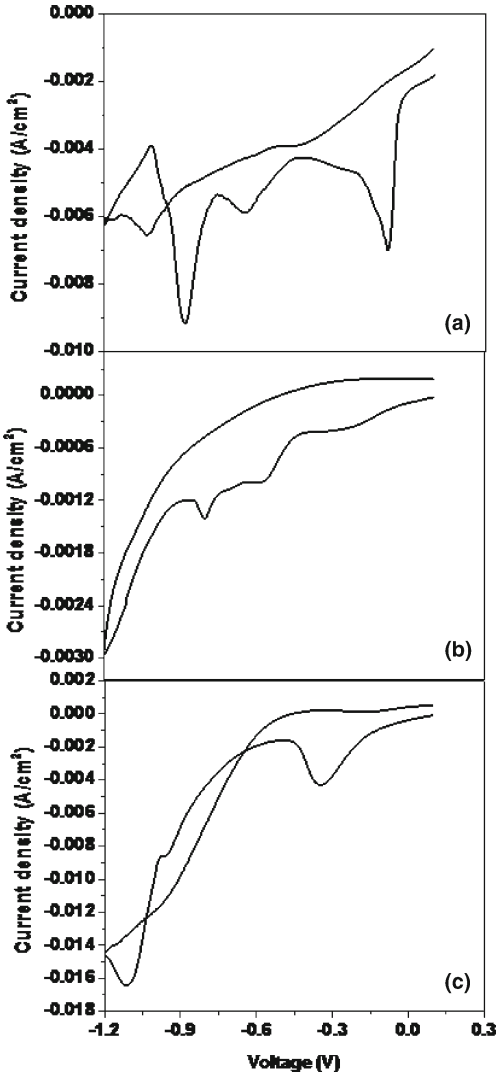

Figure 2. Voltammograms of (**a**) solution containing 20 mM $CuCl_2$ and 20 mM H_2SeO_3; (**b**) solution containing 30 mM $InCl_3$ and 20 mM H_2SeO_3 and (**c**) solution containing 40 mM $Ga(NO_3)_3$ and 20 mM H_2SeO_3.

$$3Se + 2In^{3+} + 6e^- \leftrightarrow In_2Se_3. \quad (10)$$

For the case of voltammogram of binary Ga–Se system, we only see one peak at −0·3 V which corresponds to the reduction of H_2SeO_3 directly to Se and one peak at −0·95 V which corresponds to the reduction of Ga^{3+} to Ga. It means that the underpotential deposition of gallium as gallium selenides do not occur in this system. Furthermore, the presence of Ga^{3+} in the solution has inhibited the complex process described by (4) and (5).

3.3 *Voltammogram of quaternary Cu–In–Ga–Se*

Figure 3 is the voltammogram for solution containing 20 mM $CuCl_2$, 40 mM $Ga(NO_3)_3$, 30 mM $InCl_3$ and 20 mM H_2SeO_3. Again, we can observe a peak at −0·1 V which should be assigned to the formation of a Cu–Se phase as described above. We can also see a weak peak at −0·9 V which should correspond to the reduction of Ga^{3+} to Ga and/or the complex reduction of H_2SeO_3. The most notable feature in this voltammogram is a strong peak at −0·5 V. This peak may relate to one of the underpotential depositions described by (6) or (10). It is not easy to distinguish well which process this peak corresponds to. In order to elucidate this problem, further studies are needed. However, we can say that the underpotential deposition mechanism of Cu–Se and In–Se phases has occurred. This voltammogram also reveals that deposition of Ga still needs a highly negative potential.

3.4 *Potential dependence of composition*

EDS composition of the CIGS films deposited at various potentials is listed in table 1. Generally, the potential dependence of the composition is in accordance with the CV results. First of all, the concentration of Cu increases as the deposition potential decreases to −0·5 V, then decreases as the deposition potential decreases continuously. The maximum value of Cu concentration at −0·5 V should associate to the reduction process of Cu^{2+} to Cu^0 at −0·4 V (2) as well as to the low concentration of In and Ga in the samples deposited at potentials less negative than −0·5 V.

Concerning the Ga concentration, we can see that it has very low value in the samples deposited at the negative potential above −0·7 V, then rises rapidly as the potential decreases and reaches to a maximum value of 18·14% at the potential of −1·0 V. This trend in variation of Ga concentration can be expected from the CV data which show the reduction of Ga at −0·9 V. In the case of In, the insertion of

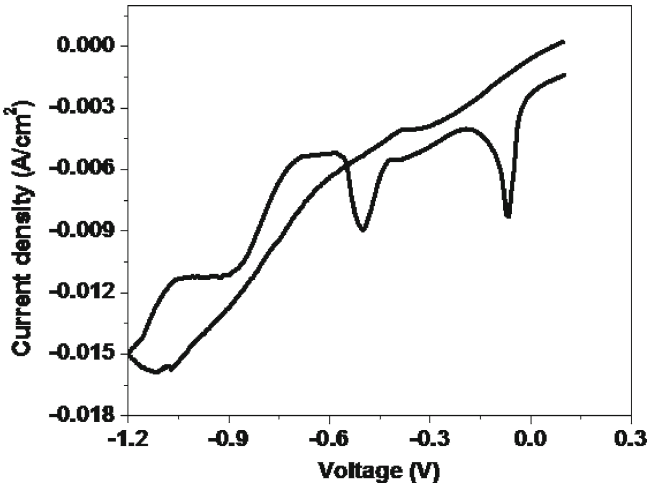

Figure 3. Voltammogram of solution containing 20 mM $CuCl_2$, 30 mM $InCl_3$, 40 mM $Ga(NO_3)_3$ and 20 mM H_2SeO_3.

In can be achieved at −0·5 V, that is more positive than the desired deposition potential for Ga. This feature may have two reasons, the reduction potential of In^{3+} to In is more positive than that for the reduction of Ga^{3+} to Ga and the underpotential deposition of indium as indium selenides occurs in the co-electrodeposition of In and Se.

Se concentration is high in all samples and depends mainly on the concentration of the other constituents. This result reveals that the deposition of Se can take place at the whole range of the investigated potential. We can expect this phenomenon from the facts that Se has two wide reduction peaks and the ability to form an intermediate phase with other constituents by underpotential deposition mechanism. It is interesting to note that there is a range of potentials from −0·8 to −1·0 V where the concentration of all the constituents is quite unaffected by the potential. This potential range is also where we can obtain the highest concentration of In and Ga. It means that this potential range is the best choice for obtaining films with desired and stable stoichiometry. Our observation about the suitable potential range is in agreement with that reported by Lai *et al* (2009).

Since CIGS films deposited by electrodeposition generally need an annealing process, evaluation of composition of the films after annealing is necessary. Three samples deposited at −0·8, −0·9 and −1·0 V were annealed in Ar at 550 °C for 60 min. We chose these samples because we considered that they were the best ones in terms of In and Ga concentrations. EDS composition of these films are listed in table 2. We can

Table 1. EDS composition of CIGS films deposited at various potentials.

Potential (V vs Ag/AgCl)	Atomic percent (%) Cu	In	Ga	Se	Stoichiometry
−0·3	23·9	03·3	01·9	70·9	$CuIn_{0.14}Ga_{0.08}Se_{2.96}$
−0·4	25·7	04·6	02·0	67·7	$CuIn_{0.18}Ga_{0.08}Se_{2.63}$
−0·5	27·0	10·2	02·3	60·5	$CuIn_{0.37}Ga_{0.08}Se_{2.24}$
−0·6	22·7	16·5	02·9	57·9	$CuIn_{0.73}Ga_{0.13}Se_{2.56}$
−0·7	19·8	19·5	06·0	54·7	$CuIn_{0.98}Ga_{0.30}Se_{2.76}$
−0·8	18·2	23·7	08·7	49·4	$CuIn_{1.30}Ga_{0.47}Se_{2.70}$
−0·9	18·0	22·4	13·4	46·2	$CuIn_{1.24}Ga_{0.74}Se_{2.56}$
−1·0	17·5	22·1	14·1	46·3	$CuIn_{1.26}Ga_{0.80}Se_{2.64}$
−1·1	17·0	21·8	13·2	48·0	$CuIn_{1.28}Ga_{0.77}Se_{2.81}$

Table 2. EDS composition of post-annealed films deposited at −0·8, −0·9 and −1·0 V from electrolyte bath containing 20 mM $CuCl_2$, 30 mM $InCl_3$, 40 mM $Ga(NO_3)_3$ and 20 mM H_2SeO_3.

Potential (V vs Ag/AgCl)	Atomic percent (%) Cu	In	Ga	Se	Stoichiometry
−0·8	19·5	25·2	09·5	45·8	$CuIn_{1.29}Ga_{0.48}Se_{2.35}$
−0·9	19·4	23·6	13·8	43·2	$CuIn_{1.22}Ga_{0.71}Se_{2.23}$
−1·0	18·7	23·5	14·3	43·5	$CuIn_{1.25}Ga_{0.76}Se_{2.32}$

see that the most significant difference between the composition of these films and those of as-deposited films is the decrease in Se content. This difference is due to the higher evaporation rate of Se compared to those of Cu, In and Ga.

Table 3. EDS composition of post-annealed films deposited at −0·8, −0·9 and −1·0 V from electrolyte bath containing 20 mM $CuCl_2$, 20 mM $InCl_3$, 30 mM $Ga(NO_3)_3$ and 20 mM H_2SeO_3.

Potential (V vs Ag/AgCl)	Atomic percent (%)				Stoichiometry
	Cu	In	Ga	Se	
−0·8	25·5	17·7	6·2	50·6	$CuIn_{0.69}Ga_{0.24}Se_{1.98}$
−0·9	24·8	16·9	9·6	48·7	$CuIn_{0.68}Ga_{0.38}Se_{1.96}$
−1·0	24·2	15·6	10·5	49·7	$CuIn_{0.64}Ga_{0.43}Se_{2.05}$

On noting that the main deviation of the composition of these films from the desired stoichiometry of $Cu(In_{0.7}Ga_{0.3})Se_2$ was the high concentration of In and Ga, and we deposited the other three films, also at the potentials of −0·8, −0·9 and −1·0 V, but from a new electrolyte bath and which contained 20 mM $CuCl_2$, 20 mM $InCl_3$, 30 mM $Ga(NO_3)_3$ and 20 mM H_2SeO_3. The films were also annealed in Ar at 550 °C for 60 min. EDS composition of these films after annealing are listed in table 3, showing clearly an improvement in matching the desired stoichiometry.

3.5 *Morphology and crystallinity*

Figure 4 is the cross-sectional and surface morphology (SEM) of typical as-deposited samples, namely, the ones deposited at −0·3, −0·6 and −0·9 V. As seen, these

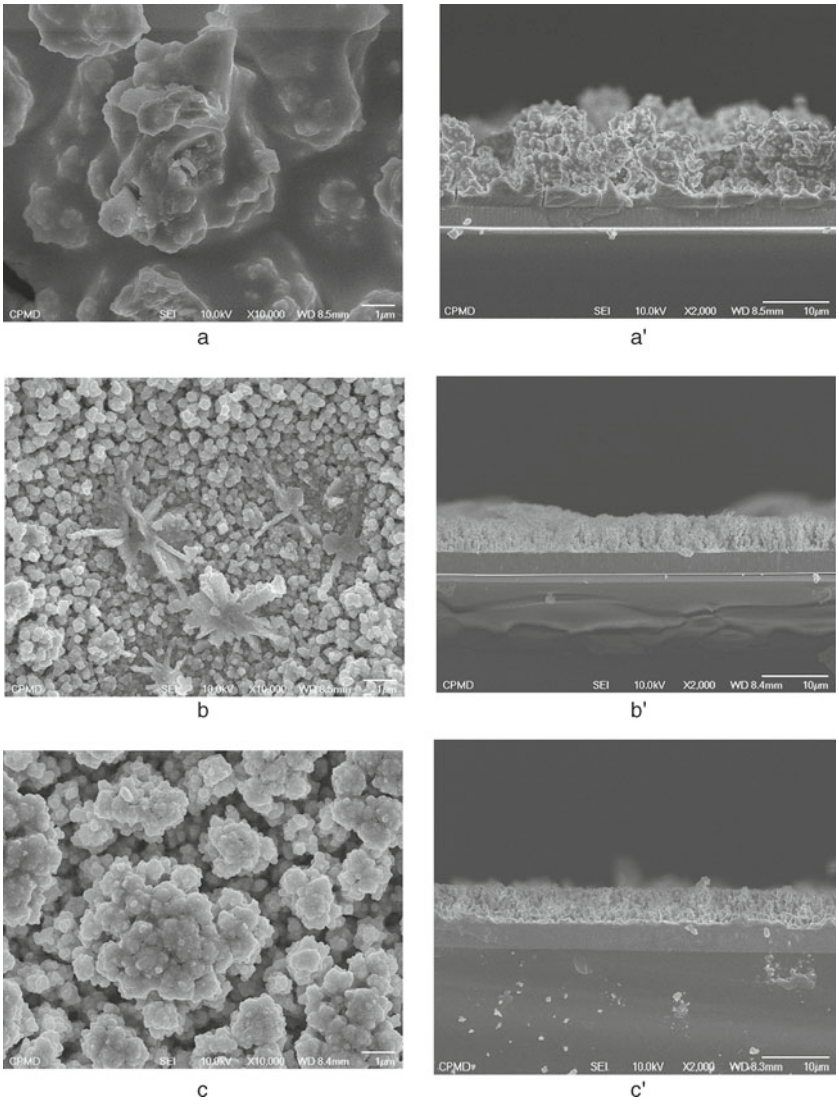

Figure 4. Cross-sectional and surface morphology (SEM) of typical as-deposited samples deposited at (a, a′) −0·3 V, (b, b′) −0·6 V and (c, c′) −0·9 V vs Ag/AgCl.

films have poor crystallinity with porous, non-uniform and polyphasic structure. However, these micrographs also indicate that the samples deposited at less negative potential are more dense and compact. This is because these samples consist mainly of the phases containing Cu and Se.

The effect of annealing process on the morphology and crystallinity of the samples can be seen in figure 5. We can see clearly that these films are more dense and compact. The most significant difference between the as-deposited and the post-annealed films is the change in the shape of the grains, i.e. from cauliflower-like to flake-like. This is a clear evidence of crystallization occurring during annealing process.

Evolution of morphology and crystallinity under the variation of applied potential and the annealing process can be seen more from the XRD results which are shown in figure 6. In all cases of as-deposited samples, XRD patterns exhibit a nanocrystalline and/or amorphous structure. For that reason, we show only one pattern of a typical as-deposited sample. XRD patterns of the post-annealed samples reveal that these films have a better crystalline structure. Typical peaks of the chalcopyrite structure, viz. (112), (220) and (312) start appearing in the XRD pattern of the sample deposited at −0·5 V, the intensity of these peaks increases with the change in applied potential towards negative direction and then becomes strongly dominant in the XRD pattern of the film deposited at −0·9 V. In the XRD pattern of this film (pattern d), we can also see some very weak peaks. However, these peaks can still be identified as the peaks of chalcopyrite structure and are indexed

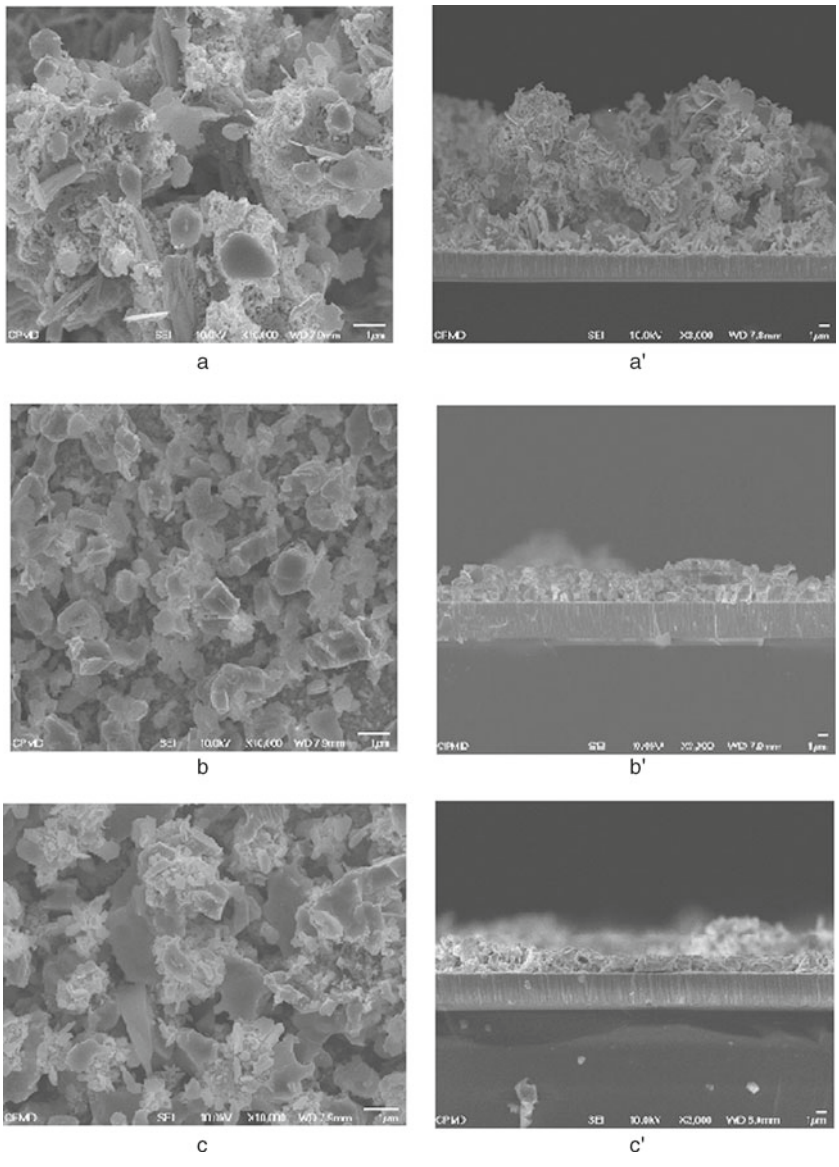

Figure 5. Cross-sectional and surface morphology (SEM) of samples deposited at (a, a′) −0·3 V, (b, b′) −0·6 V and (c, c′) −0·9 V vs Ag/AgCl, followed by annealing process at 550 °C for 60 min.

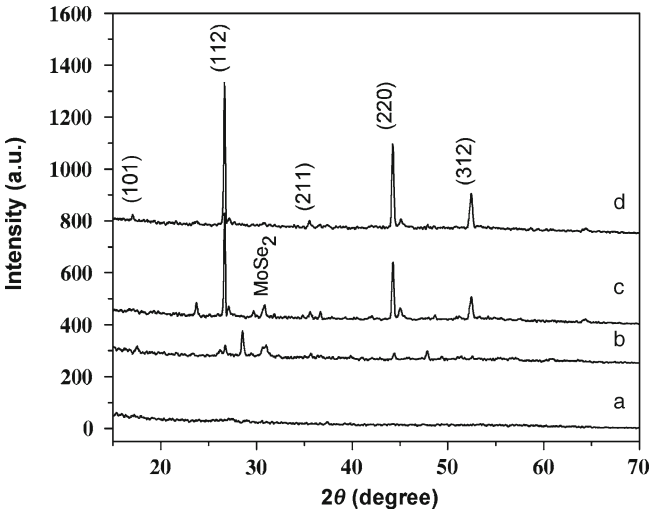

Figure 6. XRD patterns of typical CIGS films with plane indices corresponding to chalcopyrite structure: (**a**) as-deposited, post-annealed films grown at (**b**) −0·3 V, (**c**) −0·5 V and (**d**) −0·9 V vs Ag/AgCl.

in figure 6. XRD patterns of the films deposited at −0·3 and −0·5 V (patterns b and c) contain an additional peak at 31°, which belongs to $MoSe_2$ structure. $MoSe_2$ phase was formed in these films during annealing process due to the exceeding concentration of Se.

4. Conclusions

In this study, we have studied the deposition mechanism of the CIGS layer by using the cyclic voltammetry technique. We have also studied the dependence of composition on the deposition potential. Variation of concentration of each constituent was found to be in good agreement with CV data. The underpotential deposition mechanism of Cu–Se and In–Se phases was observed in voltammograms of binary and quaternary systems. A suitable potential range from −0·8 to −1·0 V and an appropriate concentration of electrolyte bath were found for obtaining films with desired and stable stoichiometry. Further studies are still needed for better understanding of CIGS layer deposition as well as for improvement in the sample morphology.

Acknowledgement

This work was supported by project NAFOSTED 103.02.59.09.

References

Abrantes I M, Araujo L V and Veli D 1995 *Miner. Eng.* **8** 1467
Bhatacharya R N, Batchelor W, Grannata J E, Hasoon H, Wiensner H, Ramanathan K, Keane J and Noufi R N 1998 *Sol. Energy Mater. Sol. C.* **55** 83
Bhatacharya R N, Hiltner J F, Batchelor W, Contreras M A, Noufi R N and Sites J R 2000 *Thin Solid Films* **361** 396
Fernandez A M and Bhatacharya R N 2005 *Thin Solid Films* **474** 10
Friedfeld R, Raffelle R D and Mantovani J G 1999 *Sol. Energy Mater. C.* **58** 375
Ganchev M, Kois J, Kaelin M, Bereznev S, Tzvetkova E, Volubuzeva O, Stratieva N and Tiwari A 2006 *Thin Solid Films* **511–512** 325
Hermann A M, Wesfall R and Wind R 1998 *Sol. Energy Mater. C.* **52** 355
Kampmann A, Sittinger V, Rechid J and Reineke-Koch R 2000 *Thin Solid Films* **361–362** 309
Kampmann A, Rechid J, Raitzig A, Wulff S, Mihhalova M, Thyen R and Kaberlah K 2003 *Mater. Res. Soc. Symp. Proc.* **763** 323
Kang F, Ao J, Sun G, He Q and Sun Y 2010 *Curr. Appl. Phys.* **10** 886
Lai Y, Liu F, Zhang Z, Liu J, Li Y, Kuang S, Li J and Liu Y 2009 *Electrochim. Acta* **54** 3004
Liu J, Liu F, Lai Y, Zhang Z, Li J and Liu Y 2011 *J. Electroanal. Chem.* **651** 191
Massaccesi S, Sanchez S and Vedel J 1996 *J. Electroanal. Chem.* **412** 95
Mishra K K and Rajeshwar K 1989 *Electroanal. Chem.* **271** 279
Repinst L, Contreras M A, Egaas B, Hart C De, Scharf J, Perkins C L, To B and Noufi R 2008 *Prog. Photovolt. Res. Appl.* **16** 235
Thouin L, Rouquette-Sanchez S and Vedel J 1993 *Electrochim. Acta* **38** 2387
Zank J, Mehlin M and Fritz H P 1996 *Thin Solid Films* **286** 259
Zhang L, Jiang F D and Feng J Y 2003 *Sol. Energy Mater. C.* **80** 483